

Special  
Collection

# Morphology-Dependent Influences on the Performance of Battery Cells with a Hierarchically Structured Positive Electrode\*\*

Johanna Naumann,<sup>\*,[a]</sup> Nicole Bohn,<sup>[a]</sup> Oleg Birkholz,<sup>[b]</sup> Matthias Neumann,<sup>[c]</sup> Marcus Müller,<sup>[a]</sup> Joachim R. Binder,<sup>[a]</sup> and Marc Kamlah<sup>\*,[a]</sup>

The rising demand for high-performing batteries requires new technological concepts. To facilitate fast charge and discharge, hierarchically structured electrodes offer short diffusion paths in the active material. However, there are still gaps in understanding the influences on the cell performance of such electrodes. Here, we employed a cell model to demonstrate that the morphology of the hierarchically structured electrode determines which electrochemical processes dictate the cell

performance. The potentially limiting processes include electronic conductivity within the porous secondary particles, solid diffusion within the primary particles, and ionic transport in the electrolyte surrounding the secondary particles. Mitigating these limits requires an electronic conductivity in the active material of at least  $10^{-4} \text{ Sm}^{-1}$  and a primary particle radius below 100 nm. Our insights enable a goal-oriented tailoring of hierarchically structured electrodes for high-power applications.

## Introduction

The ongoing transition of the energy and transport sector amplifies the requirements on batteries. Fast charging and acceleration of electric vehicles depends on the rate capability of battery cells. One approach to improve the rate capability is the hierarchical structuring of the positive electrode as depicted in Figure 1(a). In this case, the secondary active material particles consist of smaller primary particles, where the pores within the secondary particles contain electrolyte, see Figure 1(b). Compared to a conventional electrode setup, the electrochemically active surface area of the electrode enlarges and transport paths in the active material shorten. The latter has shown to increase the specific capacity especially at high insertion and extraction rates.<sup>[1,2]</sup> The performance of the cell

depends on the morphology of the hierarchically structured electrode including the microstructure of the secondary particles.<sup>[3]</sup> Despite first experimental studies, the structure-property relationships in hierarchically structured electrodes are not fully understood. Although incorporating the same electrochemical processes as conventional electrode structures, the hierarchical structure affects the interrelation of these processes and additionally requires electronic and ionic transport within the secondary particle. During manufacturing, setting different morphological properties is often interrelated, so separating their influence by individual adjustment remains difficult. Furthermore, experimentally extracting the interplay of morphology and material properties takes great effort. It requires the investigation of a wide range of materials and statistically correlating their inherent characteristics.

To complement experimental investigations, porous secondary particles for battery electrodes have been modeled by several groups. Combining experiments with 3D imaging and statistical image analysis, Wagner et al.<sup>[3]</sup> studied structure-property relationships of hierarchically structured electrodes. Moreover, Neumann et al.<sup>[4]</sup> used stochastic nanostructure modeling and numerical simulations to quantitatively investigate effective ionic and electronic transport in secondary active material particles with a designed inner porosity. Wu et al.<sup>[5]</sup> employed a continuum model of a single secondary particle concentrating on intercalation-induced stresses. Cernak et al.<sup>[6]</sup> spatially resolved the secondary particle to investigate the effect of secondary particle porosity on the cell performance. Lueth et al.<sup>[7]</sup> developed a continuum cell model for electrodes which consist of secondary particles possessing a certain inner porosity due to their agglomerate character. With this model, they studied the dependence of cell performance on two morphological and two material properties. Namely, they considered effects of the electrochemically active surface area, the secondary particle porosity, the diffusivity in the active

[a] J. Naumann, N. Bohn, Dr. M. Müller, Dr. J. R. Binder, Prof. Dr. M. Kamlah  
Institute for Applied Materials, Karlsruhe Institute of Technology  
D-76344 Eggenstein-Leopoldshafen, Germany  
E-mail: johanna.naumann@kit.edu  
marc.kamlah@kit.edu

[b] Dr. O. Birkholz  
APL Automobil-Prüftechnik Landau GmbH  
Am Hölzel 11, D-76829 Landau in der Pfalz, Germany

[c] Dr. M. Neumann  
Institute of Stochastics, Ulm University  
D-89069 Ulm, Germany

[\*\*] A previous version of this manuscript has been deposited on a preprint server (DOI: <https://arxiv.org/abs/2307.02870>)

Supporting information for this article is available on the WWW under <https://doi.org/10.1002/batt.202300264>

This publication is part of a joint Special Collection dedicated to Post-Lithium Storage, featuring contributions published in *Advanced Energy Materials*, *Batteries & Supercaps*, and *ChemSusChem*.

© 2023 The Authors. *Batteries & Supercaps* published by Wiley-VCH GmbH. This is an open access article under the terms of the Creative Commons Attribution License, which permits use, distribution and reproduction in any medium, provided the original work is properly cited.

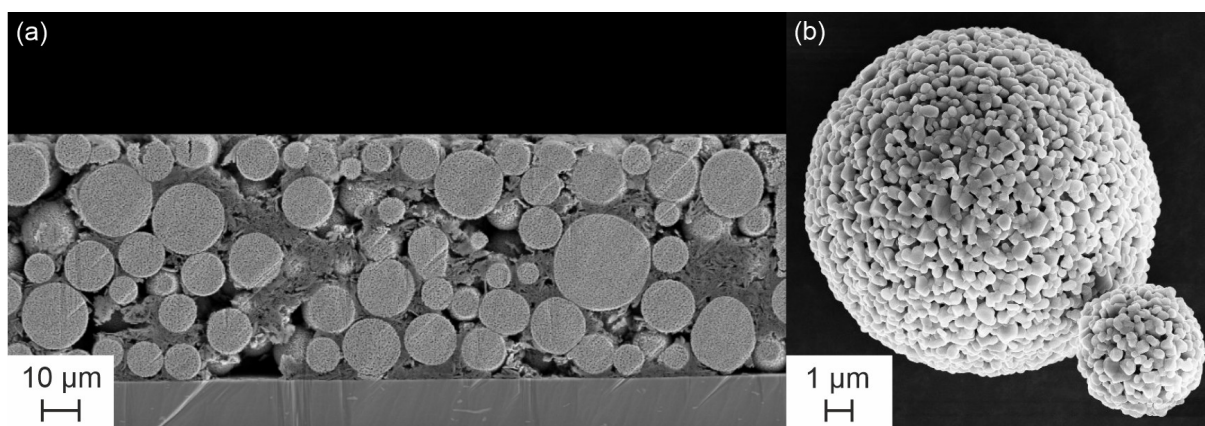


**Figure 1.** SEM images: a) Cross-section of hierarchically structured electrode E2 with 73  $\mu\text{m}$  thickness. b) Secondary particle of comparable powder to F900 from Wagner et al.<sup>[3]</sup>

material, and the electronic conductivity of the active material. Birkholz et al.<sup>[8]</sup> applied a similar model to hierarchically structured electrodes with designed inner porosity of the secondary particles. They quantified the influence of diffusivity and electronic conductivity on the rate capability of the cell. However, systematic model-based investigations of the relationship between electrode morphology, material properties, and cell performance across all scales in hierarchically structured electrodes have not been performed so far.

Here, we combined a continuum cell modeling framework with experimental investigations to show that different processes in the battery cell influence its performance depending on the morphology and material properties of the hierarchically structured positive electrode. We determined the change in rate capability in terms of specific capacity with a variety of morphological features as well as their interplay with material properties. Under different conditions, different physical processes within the cell limit its rate capability. From these findings, we deduced recommendations for the design of hierarchically structured electrodes. Our investigations extend the work of Birkholz et al.<sup>[8]</sup> including a refined parameter set, see Supporting Information section “Properties of the E1 reference cell”. To the best of our knowledge, we are the first group to correlate the influence of morphology and material properties in hierarchically structured electrodes within a cell model. Our contribution provides a basis for a more intentional development of hierarchically structured electrodes.

## Experimental

### Experimental details

To compare the modeled data with experimental data, we prepared powders with different secondary particle porosity, electrochemically active surface area, and primary particle size. For this, we milled a commercially available  $\text{LiNi}_{1/3}\text{Mn}_{1/3}\text{Co}_{1/3}\text{O}_2$  (NMC111) powder (NM-3100, Toda America) in an agitator bead mill with different grinding media sizes (0.2 mm and 0.1 mm) and spray dried it to form spherical secondary particles. Afterwards we sintered the two

powders at different temperatures (A and B: 800 °C for 5 h, C: 850 °C for 5 h and D: 800 °C for 1 h and 700 °C for 10 h) under air to adjust the primary particle size and porosity (Figure 2).

We characterized all powders as follows: Secondary particle size by laser diffraction, electrochemically active surface area by BET-method with  $\text{N}_2$  adsorption, secondary particle porosity by mercury intrusion, and primary particle size by FE-SEM investigations in combination with image analysis. The detailed processing route and powder characterization was described in Wagner et al.<sup>[3]</sup> and Dreizler et al.<sup>[9]</sup> The results of the porous NMC111 powders are summarized in Table 1.

For electrochemical tests, we produced electrodes by mixing NMC111 powder, PvdF binder (Solef 5130, Solvay Solexis), carbon black (Super C65, Imerys Graphite & Carbon), and graphite (KS6L Imerys Graphite & Carbon) in a 87:4:4:5 ratio (wt.%) in N-methyl-2-pyrrolidone (NMP). We doctor bladed the slurry on an aluminum current collector at 200  $\mu\text{m}$  gap height and dried it overnight at 80 °C. After drying we slightly compacted the electrodes. The properties of the electrodes are listed in Table 2. Significant

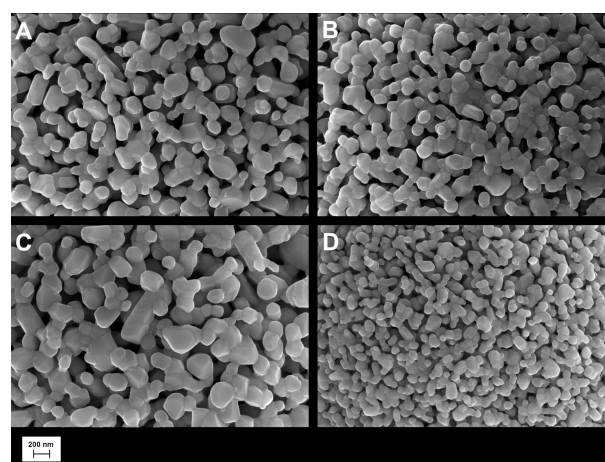


**Figure 2.** SEM images: NMC111 powders with different secondary particle porosity, electrochemically active surface area and primary particle size. Powders A and C were ground with 0.2 mm and powders B and D with 0.1 mm grinding balls. The sintering conditions of powders A and B were 800 °C for 5 h, powder C was sintered at 850 °C for 5 h, and a two-step sintering process (800 °C for 1 h and 700 °C for 10 h) was applied to powder D.

**Table 1.** Powder characteristics of the porous NMC111 materials.

Electrode	Secondary Particle Porosity [–]	Primary Particles Radius [μm]	Electrochemically Active Surface Area [m <sup>2</sup> g <sup>–1</sup> ]	Secondary Particle Radius [μm]
A	<b>0.514</b>	0.127	5.1	<b>4.5</b>
B	<b>0.439</b>	0.102	4.9	<b>3.5</b>
C	0.476	<b>0.156</b>	3.6	<b>4.8</b>
D	0.474	<b>0.072</b>	7.4	<b>3.6</b>

**Table 2.** Properties of hierarchically structured electrodes.

Electrode	Loading [mg cm <sup>–2</sup> ]	Thickness [μm]	Volume Fraction NMC111 (w/internal porosity) [–]	Electrode Porosity (w/o internal porosity) [–]	Volume Fraction Additives [–]
A <sup>[c]</sup>	7.9	48	0.3470 (0.7141)	0.5253 (0.1582)	0.1277
B <sup>[c]</sup>	7.4	45	0.3609 (0.6433)	0.5064 (0.2240)	0.1327
V <sup>[c]</sup>	7.4	43	0.3548 (0.6771)	0.5147 (0.1924)	0.1305
D <sup>[c]</sup>	8.0	50	0.3354 (0.6377)	0.5412 (0.2389)	0.1234
E1 <sup>[a,c]</sup>	8.2	<b>46</b>	0.3734 (0.5762)	0.4893 (0.2865)	0.1373
E2 <sup>[b,d]</sup>	12.4	<b>73</b>	0.3559 (0.5991)	0.5132 (0.2700)	0.1309
E3 <sup>[b,d]</sup>	18.6	<b>207</b>	0.3650 (0.6145)	0.5007 (0.2512)	0.1343
E4 <sup>[b,d]</sup>	22.3	<b>154</b>	0.3032 (0.5104)	0.5853 (0.3781)	0.1115

[a] Comparable powder to F900 from Wagner et al.<sup>[3]</sup> was used. [b] Powder from Dreizler et al.<sup>[9]</sup> was used. [c] Electrochemical testing was performed using CR2032 coin-type cells. [d] Electrochemical testing was performed using Swagelok-type cells.

variations in single properties are highlighted in Table 1 and Table 2. The following sections describe their effect on the cell performance.

From the prepared electrodes, a Whatman GF/C separator, electrolyte (LP30), and a lithium metal negative electrode we built Swagelok-type and CR2032 coin-type cells. For electrochemical testing we used a BT2000 battery cycler from Arbin Instruments. We performed galvanostatic cycling at discharge rates of C/20, C/2, 1C, 2C, 3C, 5C, 7C, and 10C in a voltage range between 4.3–3.0 V.

### Hierarchically structured half-cell model

For our modeling studies, we used the hierarchically structured half-cell model developed by Birkholz et al.,<sup>[8]</sup> see Supporting Information section “Hierarchically structured half-cell model”. It builds on the electrochemical model for lithium-ion batteries (classical cell model) by Newman and coworkers.<sup>[10–18]</sup> Both models employ the porous electrode theory.<sup>[19–21]</sup> In this framework, potentials and concentrations within the half-cell are volume-averaged. Only the concentration in the active material is spatially resolved. The half-cell and the active material particles each represent a pseudo-dimension in the classical cell model. Birkholz et al.<sup>[8]</sup> extended the classical half-cell model to describe hierarchically structured electrodes (hierarchically structured half-cell model). For this purpose, they defined three pseudodimensions: the half-cell level, the secondary particles, and the primary particles. The hierarchically structured half-cell model incorporates the following electrochemical processes:

- Ionic mass and charge transport via the electrolyte both at half-cell level and within the secondary particles.
- Electronic transport in the solid phase both at half-cell level and within the secondary particles.
- Electrochemical reaction at the primary particle surfaces.
- Diffusion of the reduced species in the active material.

The solid phase covers the behavior of the active material and the conductive additives. We modified the hierarchically structured half-cell model in two ways. First, we assumed diffusion paths to be longer than the primary particle radius by a factor of 1.5. Schmidt et al.<sup>[22]</sup> suggested this assumption if part of the active material particle surface is blocked. This is the case for hierarchically structured electrodes, since the primary particles are sintered together. In the following and the Supporting Information,  $R^{(0)}$  denotes the representative length of the diffusion paths. Second, we decoupled the electrochemically active surface area of the electrode from other morphological properties by modifying the boundary condition at the primary particle surfaces  $r^{(0)} = R^{(0)}$ :

$$\left[ D_s^{(0)} \frac{\partial c_s^{(0)}}{\partial r^{(0)}} \right]_{r^{(0)}=R^{(0)}} = - \frac{(R^{(0)}/1.5) a_s^{(0)} \bar{j}}{3 \varepsilon_s^{(0)}} \quad (1)$$

In the original model, the concentration influx  $D_s^{(0)} \frac{\partial c_s^{(0)}}{\partial r^{(0)}}$  equals the species flux density produced by the electrochemical reaction  $\bar{j}$ . In Equation (1), we used a prefactor containing the primary particle radius  $R^{(0)}/1.5$ , the volume fraction of the active material within the secondary particles  $\varepsilon_s^{(0)}$ , and the electrochemically active surface area  $a_s^{(0)}$  to enable that they can be chosen independent of each other in a physically consistent manner. Decoupling the electrochemically active surface area from the particle radius within the classical cell model would require a similar approach using the volume fraction of active material in the electrode. We used the extended hierarchically structured half-cell model to study a hierarchically structured positive electrode in a half-cell setup under galvanostatic discharge until a cut-off voltage of 3.0 V. The corresponding differential equations and boundary conditions were solved in COMSOL Multiphysics.

### Model validation and morphology variation

As a reference cell, we chose the half-cell with the E1 electrode. Supporting Information section "Properties of the E1 reference cell" lists geometric and material properties of the reference cell. Müller et al.<sup>[2]</sup> and Schneider et al.<sup>[23]</sup> investigated similar electrodes, including charge-discharge behavior, incremental capacities (cyclic voltammograms), internal resistances (EIS), and aging behavior.

To validate the applicability of the hierarchically structured half-cell model, we compared modeled discharge curves at rates between C/20 and 5C to the experimental results. Figure 3 demonstrated their qualitatively good agreement. The model captured the general shape of the discharge curves. In addition, it reproduced the trend of decreasing specific capacity with increasing discharge rate and predicted the specific capacity with an error of  $\leq 11.7\%$ . Therefore, we considered the model appropriate to qualitatively study the reference cell and cells with similar electrodes.

With our investigations, we aimed at gaining insight into the structure-property relationships of hierarchically structured electrodes. For this purpose, we separately varied morphological properties and modeled the discharge of the cell at rates ranging from C/20 to 10C. This paper includes studies of the electrochemically active surface area, the secondary particle porosity, the secondary particle size, the primary particle size, and the electrode thickness. For each property, we identified the underlying physical processes which explained the observed behavior of the cell. Besides structural parameters, we modified material properties in order to study their interaction with morphology.

### Results and Discussion

#### Effect of electrochemically active surface area on reaction kinetics

The first goal was to quantify the influence of the electrochemically active surface area on the rate capability. Studying this property experimentally is especially difficult since in reality the electrochemically active surface area depends on primary and secondary particle size as well as on porosity. Our cell model provided a deeper understanding of these single factors by separating the effect of electrochemically active surface area on the cell performance from the other influencing factors. With an extension of the hierarchically structured half-cell model in Equation (1), we enabled a variation of the electrochemically active surface area independent from all other electrode properties. In addition to the boundary condition at the primary particle surfaces, the electrochemically active surface area affects the source terms of the hierarchically structured half-cell model (Supporting Information Equations (4–5) and (14–16)), which describe the magnitude of intercalation. The reference electrode had an electrochemically active surface area of  $7.62 \times 10^6 \text{ m}^{-1}$ . The investigated range of  $2.40 \times 10^6 \text{ m}^{-1}$  ( $0.5 \text{ m}^2 \text{ g}^{-1}$ ) to  $21.50 \times 10^6 \text{ m}^{-1}$  ( $4.5 \text{ m}^2 \text{ g}^{-1}$ ) corresponds to typical values observed in experiments.<sup>[3]</sup> Supporting Information Equation (33) gives a conversion of  $\text{m}^{-1}$ , which is required by the hierarchically structured half-cell model, to  $\text{m}^2 \text{ g}^{-1}$ , which is common in experimental contexts. Figure 4(a) showed that the

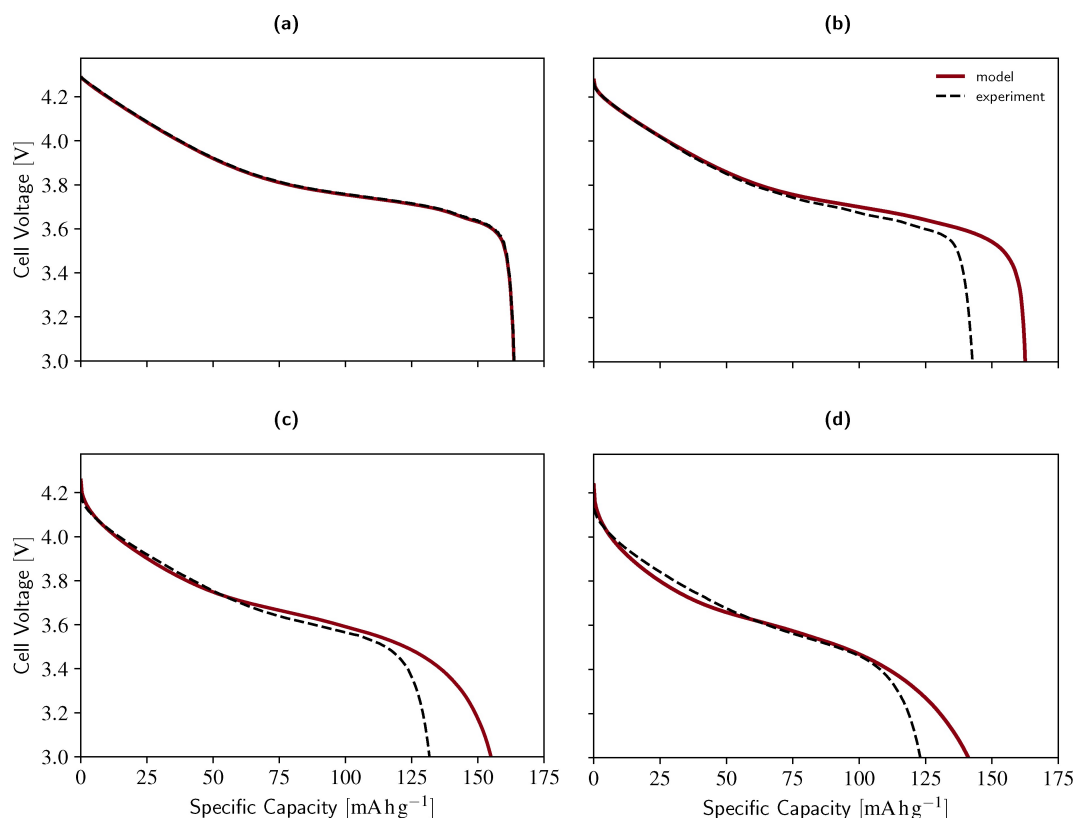


**Figure 3.** Comparison of the modeled and experimental discharge behavior of the reference cell at a) C/20, b) 1C, c) 3C, d) 5C.

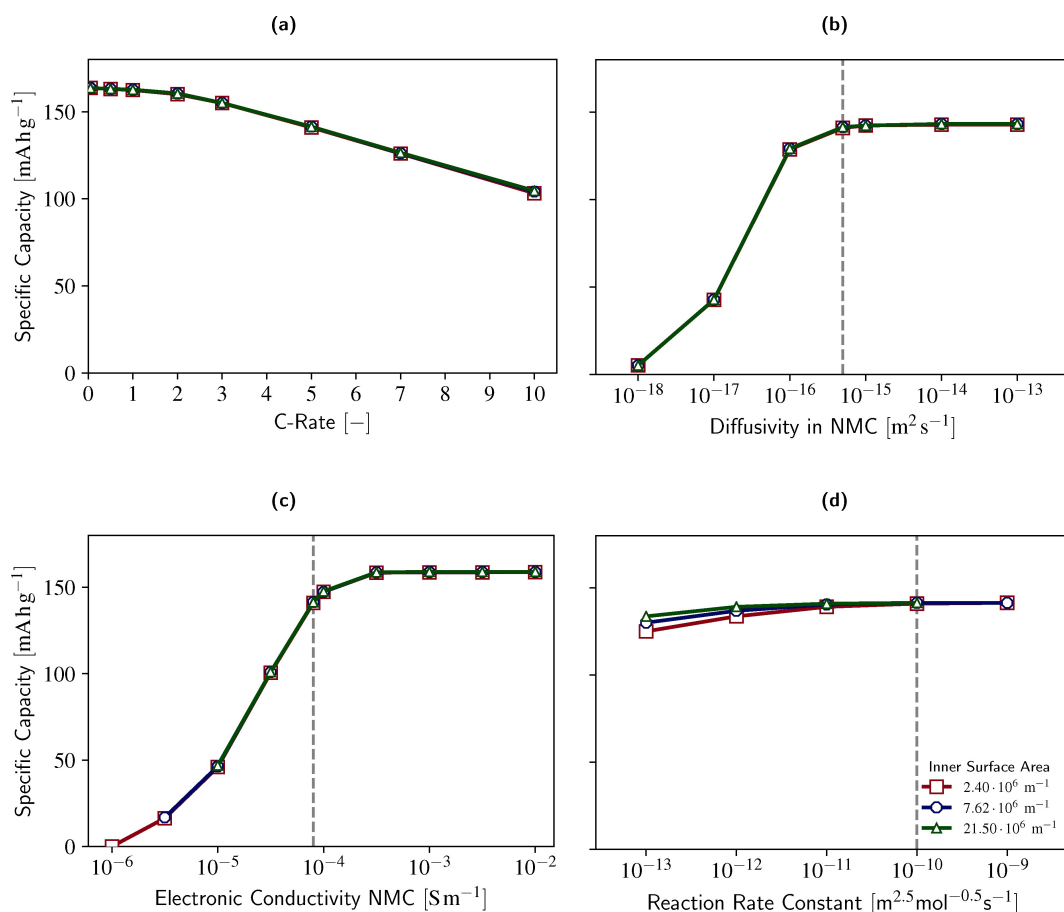


**Figure 4.** a) Rate capability of electrodes with different electrochemically active surface area. b–d) Influence of (b) diffusivity in the active material, c) electronic conductivity of the active material, d) reaction rate on the cell performance at 5C.

acquired rate capability of cells with electrodes of different electrochemically active surface area was identical. Therefore, we find that within the chosen range, the electrochemically active surface area of the electrode has no effect on the cell performance. Lueth et al.<sup>[7]</sup> found the discharge capacity of agglomerates significantly depends on the electrochemically active surface area of the electrode. At the investigated 5C discharge rate, their model yielded a constant decrease in capacity toward the end of discharge. This contrasts with the S-shaped discharge curves from our modeling results, which agreed with the experimental findings, see Figure 3. The difference in discharge profiles highly affects the obtained capacity and offers an explanation for the deviation between the two models.

To broaden our results, we studied electrodes with different material properties. Namely, we altered material properties which interdepend with the studied morphological properties, i.e. reaction rate, electronic conductivity of the active material, and diffusivity in the active material (see Supporting Information Equations (6, 16, 23)). These material properties may vary with different synthesis of the active material or processing of the electrode. Influences on the reaction rate include active material coatings and the composition of the electrolyte.<sup>[24]</sup> Electronic conduction involves the bulk of the secondary

particles<sup>[25]</sup> and therefore depends on the quality of grain boundaries. Crystal structure and lattice defects govern the diffusivity in the active material.<sup>[26,27]</sup> Figure 4(b) depicts the dependence of cell performance on the active material diffusivity at 5C as an example for a high discharge rate. For a given diffusivity, electrodes with different electrochemically active surface area yielded identical cell performance. Likewise, varying the electrochemically active surface area did not affect the influence of the electronic conductivity of the active material on the cell performance, see Figure 4(c). Only reaction rate constants lower than  $10^{-10} \text{ m}^{2.5} \text{ mol}^{-0.5} \text{ s}^{-1}$  caused a difference in rate capability as depicted in Figure 4(d). In this case, high surface area electrodes retained a higher specific capacity at 5C because the rate of the electrochemical reaction determined the cell performance. Since the deviation was small even under these extreme conditions, we conclude that hierarchically structured electrodes in general tend to be insensitive to a change in electrochemically active surface area.

### Interplay between secondary particle porosity and electronic conductivity

Next, we investigated to what extent the cell performance of hierarchically structured electrodes depends on the secondary particle porosity. For this purpose, we studied electrodes A and B, which featured differing secondary particle porosity and size but comparable primary particle size. Figure 5(a) revealed a decreasing specific capacity with increasing discharge rate. Furthermore, the capacity fade was more pronounced for electrode A containing more porous and larger secondary particles. The hierarchically structured half-cell model could separate the two influences. In this section, we first investigated the influence of secondary particle porosity on the rate capability. For this purpose, we modeled electrodes of varying secondary particle porosity. At the same time, all other electrode properties complied with the reference electrode. The secondary particle porosity enters the hierarchically structured half-cell model in three ways. It explicitly affects the ionic transport (Supporting Information Equation (14)) as well as the effective transport properties (Supporting Information Figure 2) in the secondary particle. Furthermore, it changes the applied current (Supporting Information Equations (8,9,13)) in order to be consistent with C-rate. The hierarchically structured half-cell model reproduced the general discharge and rate behavior as

shown in Figure 5(b). Hence, the modeling results could be used to qualitatively explain the processes during discharge. In addition, the model confirmed the experimental trend with respect to secondary particle porosity. More porous particles provided a lower rate capability, which explained part of the deviation between electrodes A and B.

The first step to understand why a high secondary particle porosity yielded a lower rate capability lay in locating the capacity loss within the electrode structure. Figure 6(a) displays the concentration profile in the active material at the end of 5C discharge over the electrode thickness and the secondary particle radius. Here, the normalized thickness coordinate runs from 0 at the separator to 1 at the current collector. For the normalized radial coordinate of the secondary particles at the respective thickness position, 0 denotes the particle center and 1 denotes the particle surface. Irrespective of the position within the electrode, the concentration in the active material decreased towards the center of the secondary particles. The concentration gradient intensified if the secondary particles were more porous. Corresponding to the concentration gradient, a gradient in electric potential as shown in Figure 6(b) arose within the active material close to the surface of the secondary particles. Again, the gradient aggravated with increasing porosity of the secondary particles. From this we deduced that the effective electronic conductivity within the

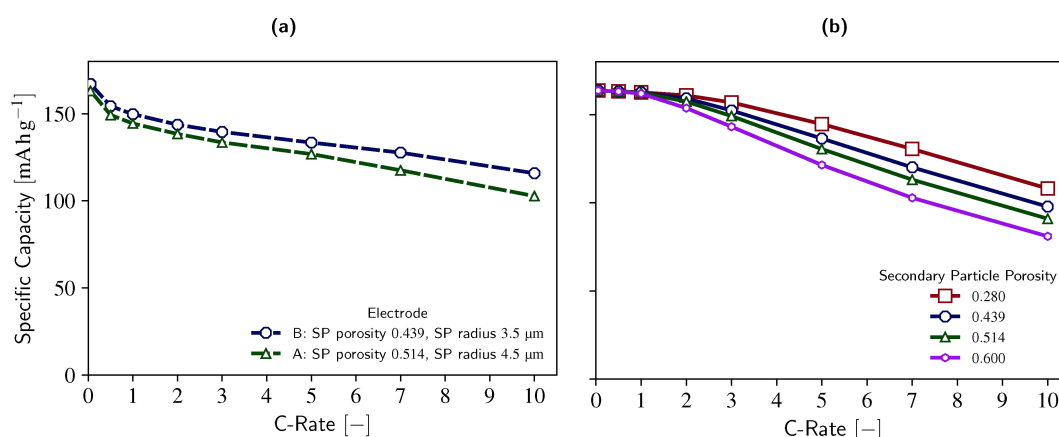


**Figure 5.** a) Experimental rate capability of electrodes A and B with differing secondary particle porosity and size, see Table 1 and Table 2. b) Modeled rate capability depending on secondary particle porosity.

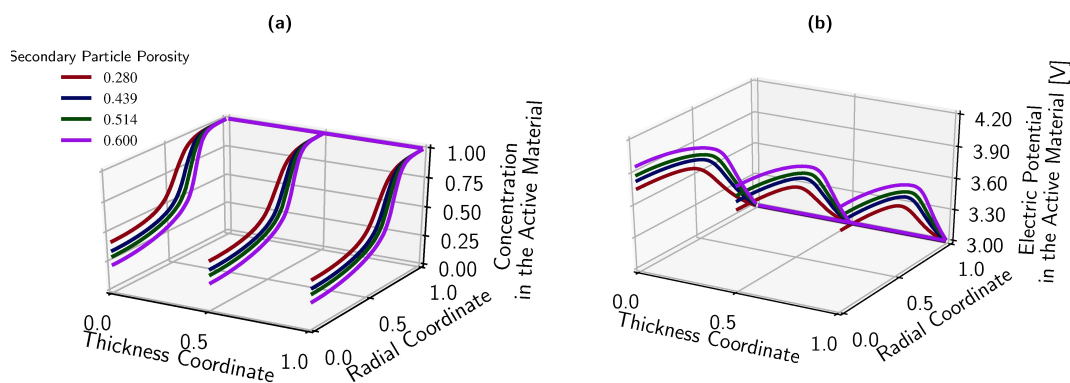


**Figure 6.** a) Normalized concentration in the active material and b) electric potential in the solid phase at the end of a 5C discharge.

secondary particles limited the cell performance. The low electronic conductivity of NMC111 caused a poor exploitation of the active material close to the center of secondary particles. As the secondary particle porosity increased, the effective electronic conductivity further declined. In consequence, low secondary particle porosities outperformed high porosities. A study of cells with varying electronic conductivity of the active material further validated our finding. Amin et al.<sup>[28]</sup> found that the electronic conductivity of NMC111 varies between  $10^{-6} \text{ S m}^{-1}$  and  $10^0 \text{ S m}^{-1}$  depending on lithiation and temperature. Furthermore, results from Kuo et al.<sup>[29]</sup> suggested that measuring the electronic conductivity of NMC111 is difficult and includes uncertainties. For this reason, we chose a range of  $10^{-6} \text{ S m}^{-1}$  to  $10^{-2} \text{ S m}^{-1}$  for studying the qualitative influence of electronic conductivity on the cell performance. As apparent in Figure 7, the cell performance scaled with the electronic conductivity in the range between  $10^{-5.5} \text{ S m}^{-1}$  and  $10^{-4} \text{ S m}^{-1}$ . Above this range, the cell performance reached a limit and other physical processes in the electrode became restrictive. Below  $10^{-5} \text{ S m}^{-1}$ , the specific capacity at 5C declined rapidly. Already at  $10^{-6} \text{ S m}^{-1}$ , the electrode ceased to deliver any capacity. Raising the electronic conductivity in the secondary particles could enhance the rate capability of the cell, which

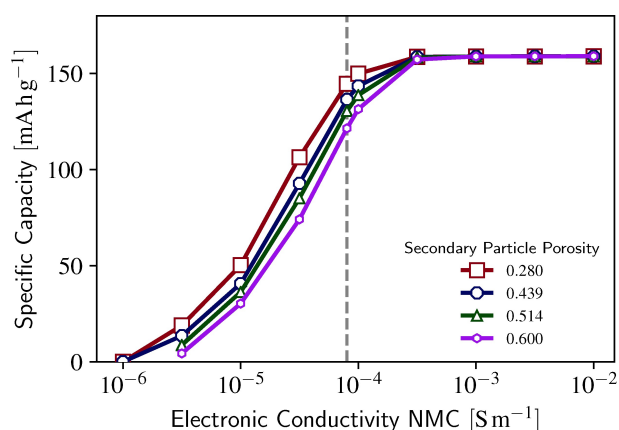


**Figure 7.** Influence of electronic conductivity within the secondary particles on the cell performance at 5C.

proves that this material property is crucial for hierarchically structured electrodes. If the electronic conductivity of the active material is poor, an enhancement of the overall electronic conductivity in the secondary particle, e.g. by carbon coating of the primary particles, is essential to ensure a good cell performance.<sup>[30,31]</sup> Our conclusions agreed with Wagner et al.,<sup>[3]</sup> Lueth et al.,<sup>[7]</sup> and Birkholz et al.,<sup>[8]</sup> who identified the electronic conductivity as a main limit for the cell performance depending on the electrode morphology.

Other material properties had less influence on the relationship between secondary particle porosity and specific capacity. The specific capacity at 5C hardly changed for diffusivities between  $10^{-16} \text{ m}^2 \text{ s}^{-1}$  and  $10^{-13} \text{ m}^2 \text{ s}^{-1}$ , see Figure 8(a). A diffusivity below  $10^{-16} \text{ m}^2 \text{ s}^{-1}$  caused the difference in cell performance at 5C to decrease. This went hand in hand with an overall drastic decrease of specific capacity for this regime, until it completely faded at  $10^{-18} \text{ m}^2 \text{ s}^{-1}$  for all values of secondary particle porosity. When altering the reaction rate constant, the difference between the cell performance remained the same, see Figure 8(b). In summary, a change in diffusivity of the active material or in reaction rate constant hardly affected how the secondary particle porosity related to the cell performance.

#### Dependence of electronic conductivity on the secondary particle size

In the previous section, we identified the electronic conductivity within the secondary particles as a limiting factor for the rate capability of hierarchically structured electrodes. Naturally, the question arose as to what extent the secondary particle size affects the performance of hierarchically structured electrodes. The secondary particle size determines the path lengths of electronic and ionic transport within the secondary particle. The hierarchically structured half-cell model includes the secondary particle size at the secondary particle level via the range of the radial coordinate  $r^{(ii)}$ , see Supporting Information Equations (14–16). In addition to a varying secondary particle porosity, the secondary particles of electrodes A and B from the previous section showed a difference in size. Electrode B with smaller

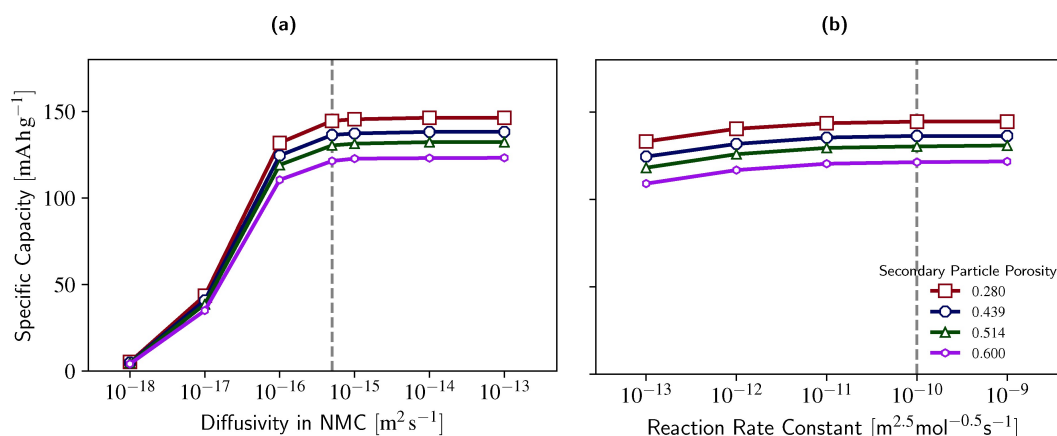


**Figure 8.** Influence of a) diffusivity in the active material and b) reaction rate on the cell performance at 5C.

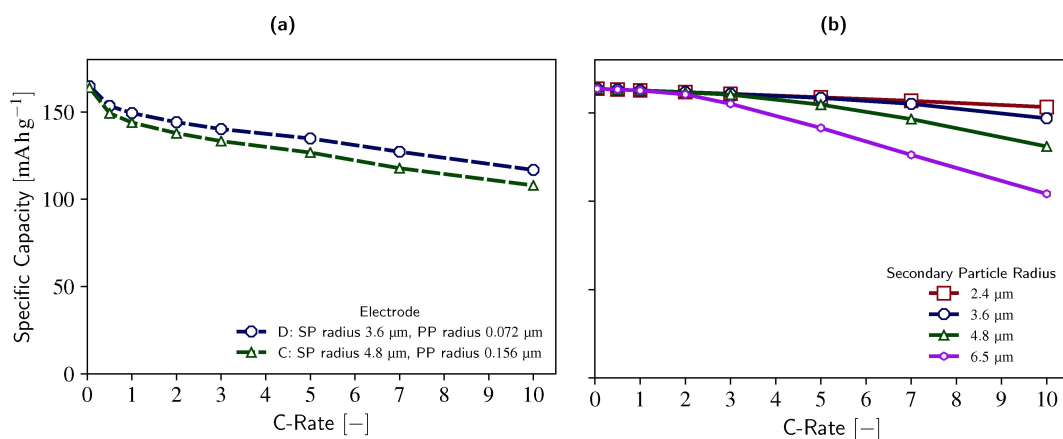


**Figure 9.** a) Experimental rate capability of electrodes C and D with differing secondary and primary particle size, see Table 1 and Table 2. b) Modeled rate capability depending on secondary particle size.

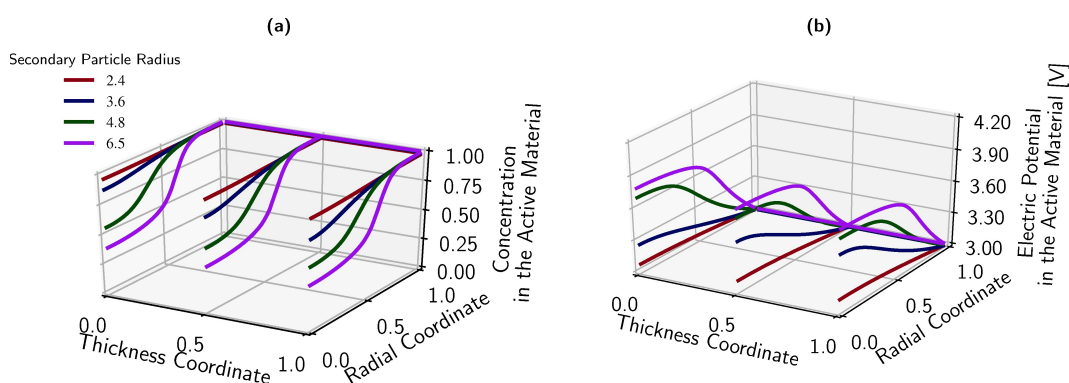


**Figure 10.** a) Normalized concentration in the active material and b) electric potential in the solid phase at the end of a 5C discharge.

and less porous secondary particles outperformed electrode A in terms of rate capability, see Figure 5(a). In addition, we considered electrodes C and D, which differed both in secondary and primary particle size. Figure 9(a) showed a higher rate capability of electrode D, consisting of smaller secondary and primary particles. Again, the hierarchically structured halfcell model could elucidate the impact of each single property. This section contains modeled results of electrodes with different secondary particle size to study its impact, while all other properties corresponded to the reference electrode. As displayed in Figure 9(b), the rate capability decreased with increasing secondary particle size. This indicated that the difference in secondary particle size could explain the difference in performance between electrodes A and B as well as between electrodes C and D to some extent. In electrodes A and B, the effects of secondary particle porosity and secondary particle size combined.

The loss in rate capability for larger secondary particles originated from an increased concentration drop over the secondary particle radius, see Figure 10(a). In the centers of large secondary particles, the active material was used to less of its capacity compared to small particles. The reason again lay in the low electronic conductivity within the secondary particles, as shown by steeper drops in electric potential with increasing

secondary particle size displayed in Figure 10(b). The long electronic transport paths to the center of large secondary particles impairs rate capability if the electronic conductivity of the active material is low.

Investigating electrodes with varying electronic conductivity in the secondary particles confirmed its relation with the secondary particle size, see Figure 11. If the electronic con-

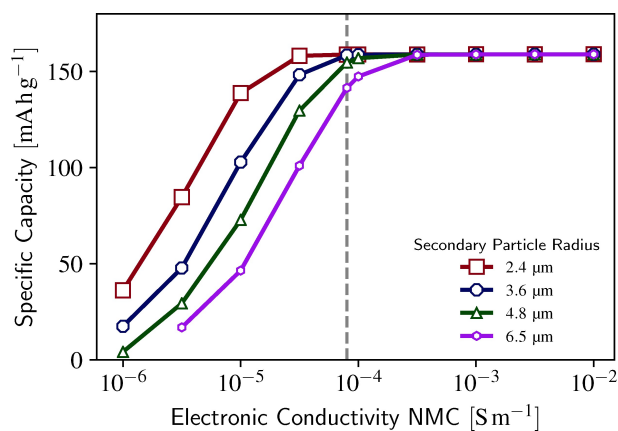


**Figure 11.** Influence of electronic conductivity within the secondary particles on the cell performance at 5C.

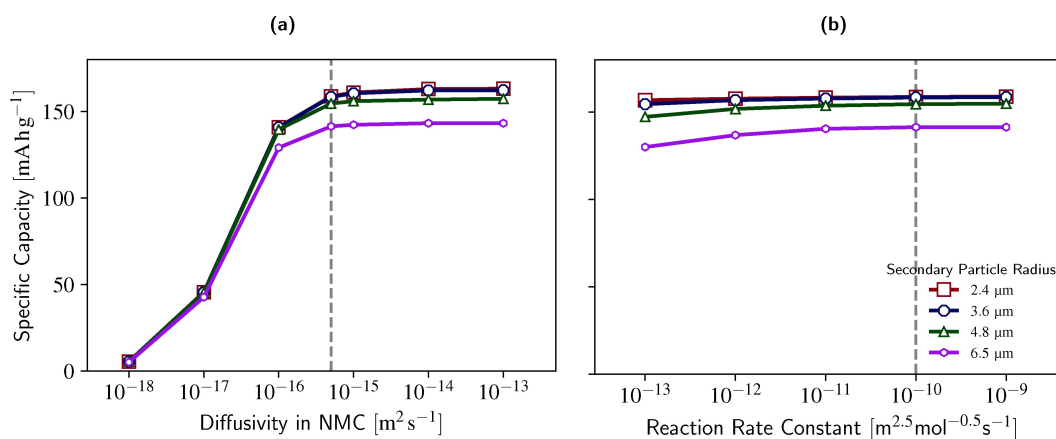


Figure 12. Influence of a) diffusivity in the active material and b) reaction rate on the cell performance at 5C.

ductivity lay between  $10^{-6} \text{ S m}^{-1}$  and  $10^{-4} \text{ S m}^{-1}$ , a larger secondary particle size significantly reduced the cell performance at high rates. Increasing the electronic conductivity raised the specific capacity at 5C from less than  $40 \text{ mAh g}^{-1}$  at the lowest electronic conductivity to a maximum of  $159 \text{ mAh g}^{-1}$  at  $10^{-3} \text{ S m}^{-1}$  or higher. For small secondary particles up to  $4.8 \mu\text{m}$  radius, an electronic conductivity of  $10^{-4} \text{ S m}^{-1}$  sufficed to ensure an optimal specific capacity. Below this electronic conductivity, the size of the secondary particles significantly governed the rate capability. Our findings deviated from Wagner et al.,<sup>[3]</sup> who reported an improved rate capability for large secondary particles. However, the compared electrodes not only differed in secondary particle size, but also in secondary particle porosity and electrode porosity. Possibly, the influence of these properties surpassed the influence of the secondary particle size.

Similar to the secondary particle porosity, the secondary particle size played a role if the diffusivity in the active material lay above  $10^{-16} \text{ m}^2 \text{ s}^{-1}$ , see Figure 12(a). For lower diffusivities, the specific capacity at 5C declined. At the same time, the behavior of electrodes with different secondary particle size assimilated. Now the diffusion in the active material limited the cell performance. Therefore the effects of the low electronic conductivity in the secondary particle lost their relevance. Figure 12(b) illustrated that the reaction rate constant barely affected the performance of electrodes with different secondary particle size.

### Limitations due to primary particle size and solid diffusion

In the previous section we showed that a difference in secondary particle size caused the rate capability of electrodes C and D to diverge. Since these electrodes also differed in primary particle size, we now studied its influence with the hierarchically structured half-cell model. The primary particle size determines the length of diffusion paths within the active material, i.e. the range of the radial coordinate  $r^{(0)}$  (Supporting Information Equation (23)). Note that after studying the electrochemically active surface area separately in section “Effect of

electrochemically active surface area on reaction kinetics”, in this section the electrochemically active surface area changed according to the primary particle size. The model shown in Figure 13 yielded a lower rate capability for large primary particles. However, the model predicted barely any difference between primary particle radii of  $0.072 \mu\text{m}$  and  $0.156 \mu\text{m}$ , which corresponded to electrodes C and D, see Figure 9(a). We concluded that the diverging secondary particle size accounted for almost all of the performance alteration between the two electrodes, while the primary particle size only contributed a small additional deviation. The primary particle size plays a role in determining the rate capability of hierarchically structured electrodes if the radius exceeds around  $0.300 \mu\text{m}$ .

The loss in rate capability due to a large primary particle size could be attributed to concentration drops inside the primary particles. Figure 14(a) depicts the difference in concentration between primary particle surfaces and centers. The increased difference for large primary particles in one specific region of the secondary particles indicated larger concentration drops due to diffusion limitations in the active material. This region lay close enough to the secondary particle surface such that it did not suffer from the poor electronic conductivity in the secondary particles. In the center of the secondary particles,

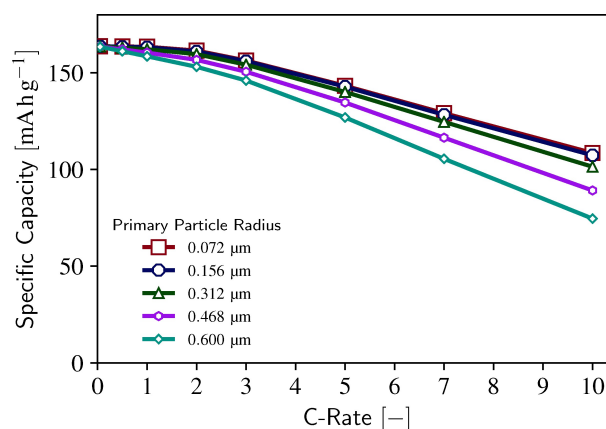
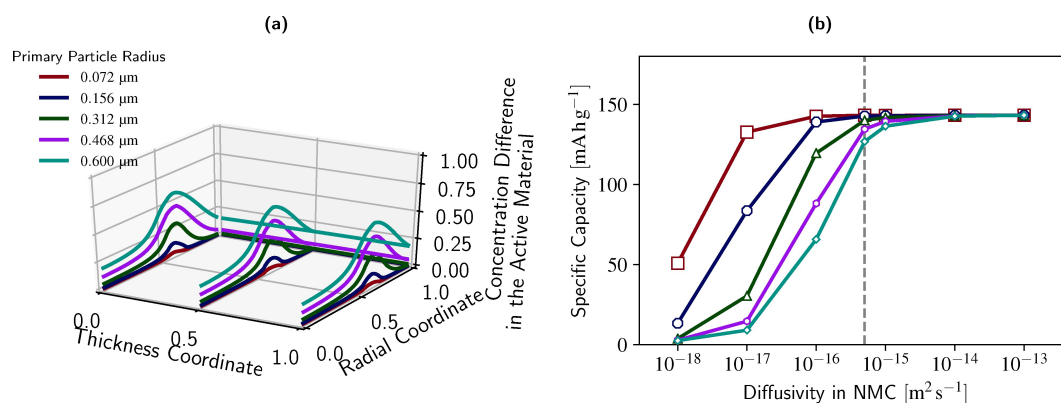


Figure 13. Modeled rate capability depending on primary particle size.



**Figure 14.** a) Difference in normalized concentration in the active material between primary particle surfaces and centers at the end of a 5C discharge. The magnitude in concentration difference indicates the magnitude in concentration drop from the surface to the center of primary particles at each position in the electrode. b) Influence of diffusivity in the active material on the cell performance at 5C.

the electronic conductivity limited the intercalation, so that the concentration was low, independent of the primary particle size.

Studies of electrodes with different diffusivity of the active material in Figure 14(b) further confirmed our explanation. Electrodes containing small primary particles with a radius of 0.072 μm remained close to the maximum performance until a diffusivity as low as 10<sup>-17</sup> m<sup>2</sup> s<sup>-1</sup>. With increasing primary particle size, the specific capacity already started dropping at higher diffusivity. At 10<sup>-18</sup> m<sup>2</sup> s<sup>-1</sup>, electrodes with primary particle radii below 0.156 μm failed completely. From this it followed that the diffusion in the active material can restrain the cell performance of hierarchically structured electrodes. Small primary particles therefore achieve the best exploitation of the active material and take full advantage of the reduced diffusion paths in hierarchically structured electrodes. In contrast to our conclusion, Birkholz et al.<sup>[8]</sup> found the cell performance to be entirely independent of the diffusivity. In comparison, we used a refined value for the diffusivity in the active material and considered diffusion paths longer than the primary particle radius. With our more realistic approach we could show that an

impact of the primary particle size is possible even in hierarchically structured electrodes.

The effect of the primary particle size intensified in magnitude after increasing the electronic conductivity of the active material in Figure 15(a). At 10<sup>-3</sup> S m<sup>-1</sup> and higher, the absolute value of the specific capacity at 5C varied more strongly between different particle sizes than for the reference electrode with 8 × 10<sup>-5</sup> S m<sup>-1</sup>. The absolute variation decreased for lower electronic conductivities while the overall cell performance diminished. At 10<sup>-6</sup> S m<sup>-1</sup>, the cell performance almost completely faded. As explained in the section "Interplay between secondary particle porosity and electronic conductivity", a low electronic conductivity of the active material can restrict the cell performance. This agrees with our finding that the primary particle size plays a more important role if the electronic conductivity of the active material is high, since this allows diffusion to become more prominent as limiting factor. Based on experimental investigations, Wagner et al.<sup>[3]</sup> also drew the conclusion that large primary particles can limit the cell performance. At low reaction rates, the impact of primary particle size slightly increased as Figure 15(b) indicated. If the maximum reaction rate dropped below 10<sup>-11</sup> m<sup>2.5</sup> mol<sup>-0.5</sup> s<sup>-1</sup>, the

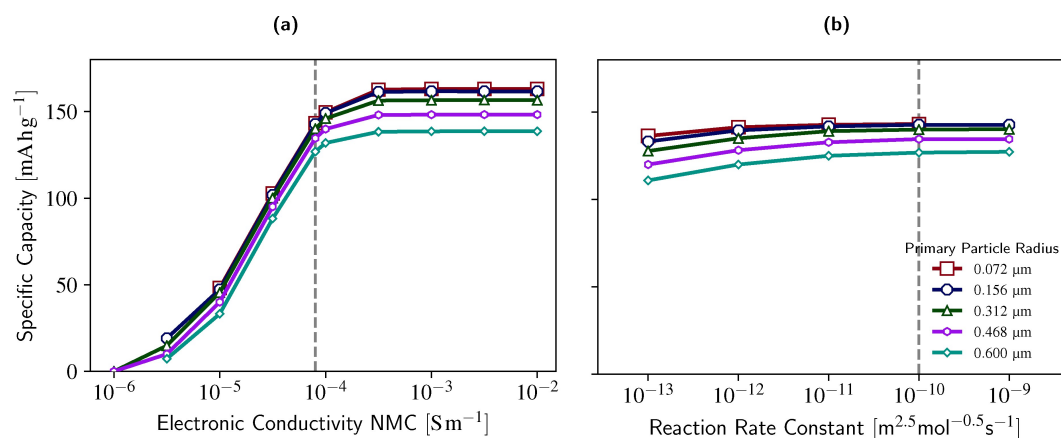


**Figure 15.** Influence of a) electronic conductivity of the active material and b) reaction rate on the cell performance at 5C.

specific capacity at 5C differed more significantly. Large primary particles imply a lower electrochemically active surface area for the same active material content of the electrode. Therefore, the electrochemical reaction slowed down, see section "Effect of electrochemically active surface area on reaction kinetics".

### Impact of ionic transport depending on electrode thickness

Finally, we investigated the electrode thickness of hierarchically structured electrodes. The hierarchically structured half-cell model incorporates the electrode thickness at the cell level (Supporting Information Equations (1–3)) by the range of the spatial coordinate  $x$ . The modeling studies depicted in Figure 16(b) displayed the same qualitative behavior as the experiment in Figure 16(a). For progressively thick electrodes the rate capability decreased. Electrodes of 107  $\mu\text{m}$  and thicker experienced a drastic drop in specific capacity within a small range of discharge rates before the decrease continued moderately above 7C.

We further investigated the reason for the changing rate capability of hierarchically structured electrodes of different thickness. For thin electrodes up to 73  $\mu\text{m}$ , Figure 17(a) revealed a general slight decrease of concentration in the active material within the secondary particles. Furthermore, at a thickness of 107  $\mu\text{m}$  a steep drop in concentration close to the current

collector occurred. Electrodes which were even thicker reached the low level of concentration across a larger portion of the thickness. As Figure 17(b) showed, the concentration drop in the active material related to a concentration drop in the electrolyte over the electrode thickness. This drop steepened with increasing electrode thickness. A lower concentration in the electrolyte caused the electrochemical reaction to run slower, so less concentration entered the active material. Electrodes of 107  $\mu\text{m}$  or thicker even experienced a complete depletion of the electrolyte in regions close to the current collector. When the electrolyte depleted, the electrochemical reaction stopped. This explained the drastically reduced concentration in the active material of these regions at the end of discharge. From our results, we deduce that the ionic transport in the electrolyte is so low that this process compromises the cell performance in thick electrodes.

For additional proof of our finding, we increased the conductivity and the diffusivity of the electrolyte by a factor of 10. This resulted in an almost identical rate capability of the cells independent of the electrode thickness, see Figure 18. Therefore, we confirmed that concentration drops in the electrolyte reduced the performance of thick electrodes. Classical electrodes with dense secondary active material particles experience the same effect.<sup>[32,33]</sup> Note that for even thicker electrodes or higher discharge rates the electronic transport through the solid phase of the electrode, which is

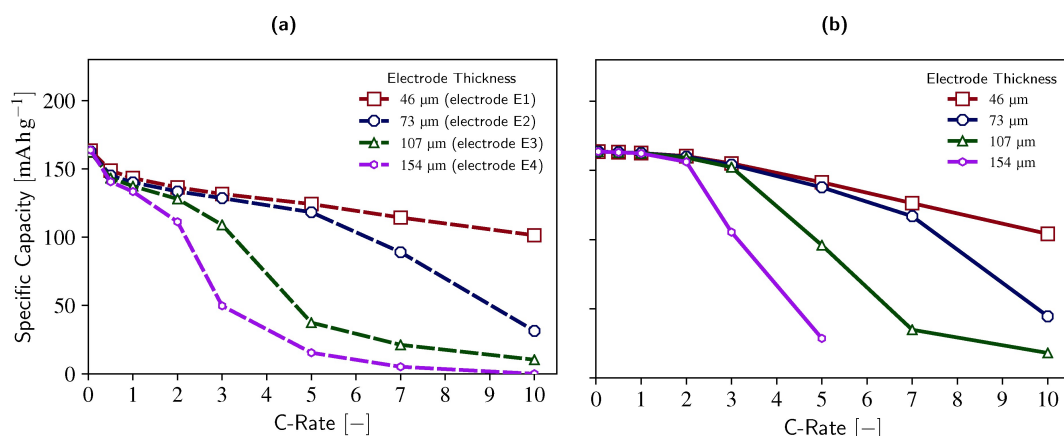


Figure 16. a) Experimental (electrode E1–4, see Table 2) and b) modeled rate capability depending on electrode thickness.

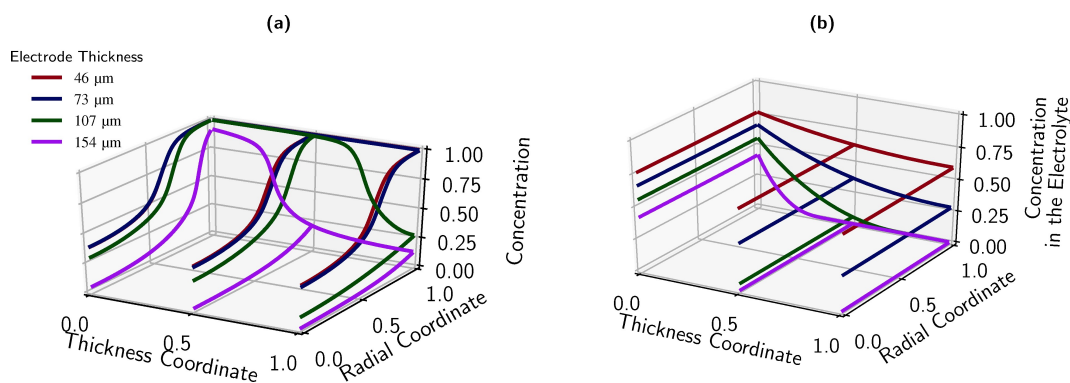
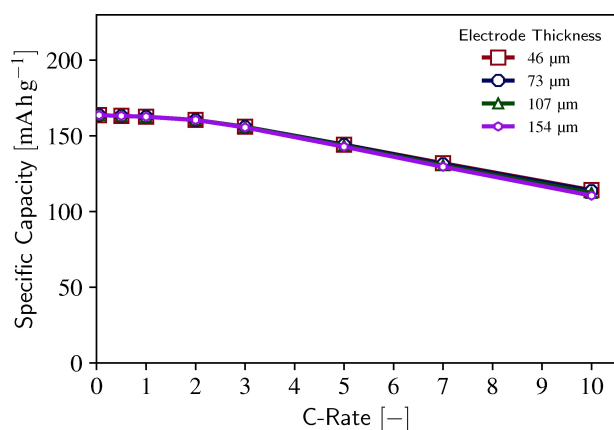


Figure 17. Normalized concentration a) in the active material and b) in the electrolyte at the end of a 5C discharge.



**Figure 18.** Rate capability when the conductivity and the diffusivity of the electrolyte are artificially increased by a factor of 10.

mainly determined by conductive additives, may become limiting.<sup>[34]</sup>

## Conclusions

Our goal was to elucidate the relationship between the morphology of hierarchically structured electrodes, material properties, and the rate capability of the cell. The hierarchically structured half-cell model provides the possibility to independently study the influence of single morphology properties and material properties, which lies beyond experimental capabilities. In addition, the model predicts local state changes and thereby tracks the electrochemical processes within the cell.

With our modeling study, we outlined the interplay between electrochemical processes within the novel concept of hierarchically structured electrodes. Electronic transport in the secondary particles is the dominant process which determines the rate capability. In case of a low electronic conductivity of the active material and no additional conductive aids inside the secondary particle, the transport of electrons to the primary particle surfaces where the electrochemical reaction takes place is insufficient. Despite the main transport taking place via conductive additives surrounding the secondary particles and comparatively short electronic transport paths within the secondary particles, the latter play a dominant role since the electronic conductivity of additives and active material differ several orders of magnitude. A low secondary particle porosity and a small secondary particle size reduce the limitations due to electronic conductivity.

Hierarchically structured electrodes rely on the small size of the primary particles for short diffusion paths. Still, the diffusion within large primary particles may limit rate capability if the diffusivity in the active material is low. Compared to conventional electrode structures the limitation is mitigated. Electrode thickness affects hierarchically structured electrodes in a similar way as classical granular electrodes consisting of dense secondary particles. Namely, with increasing thickness depletion of the electrolyte reduces the rate capability of the cell. While

transport proved to be limiting, the cell performance is insensitive to the experimentally achievable variation of electrochemically active surface area for hierarchically structured electrodes contrary to previous anticipation. This insight was enabled by separating effects of the electrochemically active surface area from primary particle size in simulations, while it is nearly impossible to vary these properties independent of each other when processing electrodes.

From our study, we deduced the following recommendations for the design of hierarchically structured electrodes. To increase the rate capability, a good electronic conductivity within the secondary particles of at least  $10^{-4} \text{ S m}^{-1}$  is crucial. In addition, if the diffusivity in the active material lies below  $10^{-15} \text{ m}^2 \text{ s}^{-1}$ , a small primary particle radius below 100 nm fully exploits the advantage of short diffusion paths in hierarchically structured electrodes. Ultrafast applications require thin electrodes, at most 70  $\mu\text{m}$ , or electrolytes with a high ion mobility. Our findings present a guideline for the design of high-performing electrodes of hierarchical structure. Conclusions for hierarchically structured electrodes were derived for NMC111 electrodes. But the general relationships between morphology, material properties, and rate capability likely apply to other systems as well, in particular for active material with poor electronic conductivity.

## Acknowledgements

This work contributes to the research performed at CELEST (Center for Electrochemical Energy Storage Ulm-Karlsruhe) and was funded by the German Research Foundation (DFG) under Project ID 390874152 (POLiS Cluster of Excellence, EXC 2154). This work has been supported by the German Federal Ministry for Economic Affairs and Climate Action (BMWK) under reference number 03ETE039J. The responsibility for the content of this publication lies with the authors. Open Access funding enabled and organized by Projekt DEAL.

## Conflict of Interests

The authors declare no conflict of interest. The funders had no role in the design of the study; in the collection, analyses, or interpretation of data; in the writing of the manuscript; or in the decision to publish the results.

## Data Availability Statement

The data<sup>[35]</sup> that support the findings of this study are openly available in Zenodo at <https://doi.org/10.5281/zenodo.8337274>, reference number 10.5281/zenodo.8337274.

**Keywords:** battery performance · ceramics · continuum model · electrode morphology · mesoporous materials

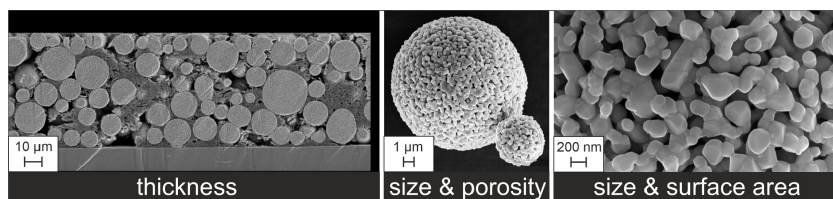
- [1] Z. Chen, J. Wang, D. Chao, T. Baikie, L. Bai, S. Chen, Y. Zhao, T. C. Sum, J. Lin, Z. Shen, *Sci. Rep.* **2016**, *6*, 1.
- [2] M. Mueller, L. Schneider, N. Bohn, J. R. Binder, W. Bauer, *ACS Appl. Energ. Mater.* **2021**, *4*, 1993.
- [3] A. C. Wagner, N. Bohn, H. Geßwein, M. Neumann, M. Osenberg, A. Hilger, I. Manke, V. Schmidt, J. R. Binder, *ACS Appl. Energ. Mater.* **2020**, *3*, 12565.
- [4] M. Neumann, S. E. Wetterauer, M. Osenberg, A. Hilger, P. Gräfensteiner, A. Wagner, N. Bohn, J. R. Binder, I. Manke, T. Carraro, V. Schmidt, *Int. J. Solids Struct.* **2023**, *280*, 112394.
- [5] B. Wu, W. Lu, *J. Electrochem. Soc.* **2016**, *163*, A3131.
- [6] S. Cernak, F. Schuerholz, M. Kespe, H. Nirschl, *Energy Technol.* **2021**, *9*, 2000676.
- [7] S. Lueth, U. S. Sauter, W. G. Bessler, *J. Electrochem. Soc.* **2015**, *163*, A210.
- [8] O. Birkholz, M. Kamlah, *Energy Technol.* **2021**, *9*, 2000910.
- [9] A. M. Dreizler, N. Bohn, H. Gesswein, M. Mueller, J. R. Binder, N. Wagner, K. A. Friedrich, *J. Electrochem. Soc.* **2018**, *165*, A273.
- [10] M. Doyle, T. F. Fuller, J. Newman, *J. Electrochem. Soc.* **1993**, *140*, 1526.
- [11] T. F. Fuller, M. Doyle, J. Newman, *J. Electrochem. Soc.* **1994**, *141*, 1.
- [12] C. M. Doyle, *Design and simulation of lithium rechargeable batteries*, Technical Report LBL-37650, Lawrence Berkeley National Lab. (LBNL), Berkeley, CA (United States) **1995**.
- [13] M. Doyle, J. Newman, *J. Power Sources* **1995**, *54*, 46.
- [14] M. Doyle, J. Newman, *Electrochim. Acta* **1995**, *40*, 2191.
- [15] M. Doyle, J. Newman, A. S. Gozdz, C. N. Schmutz, J.-M. Tarascon, *J. Electrochem. Soc.* **1996**, *143*, 1890.
- [16] M. Doyle, J. Newman, *J. Appl. Electrochem.* **1997**, *27*, 846.
- [17] M. Doyle, J. P. Meyers, J. Newman, *J. Electrochem. Soc.* **2000**, *147*, 99.
- [18] M. Doyle, Y. Fuentes, *J. Electrochem. Soc.* **2003**, *150*, A706.
- [19] J. Newman, W. Tiedemann, *AIChE J.* **1975**, *21*, 25.
- [20] K. E. Thomas, J. Newman, R. M. Darling, *Mathematical Modeling of Lithium Batteries*, in W. A. van Schalkwijk, B. Scrosati (Editors), *Advances in Lithium-Ion Batteries*, pages 345–392, Springer US, Boston, MA **2002**.
- [21] J. Newman, K. E. Thomas-Alyea, *Electrochemical Systems*, John Wiley & Sons, Inc., Hoboken, New Jersey, **2004**.
- [22] A. Schmidt, E. Ramani, T. Carraro, J. Joos, A. Weber, M. Kamlah, E. Ivers-Tiffée, *Energy Technol.* **2021**, *9*, 2000881.
- [23] L. Schneider, J. Klemens, E. C. Herbst, M. Müller, P. Scharfer, W. Schabel, W. Bauer, H. Ehrenberg, *J. Electrochem. Soc.* **2022**, *169*, 100553.
- [24] Y. Kondo, T. Abe, Y. Yamada, *ACS Appl. Mater. Interfaces* **2022**, *14*, 22706.
- [25] S. Burkhardt, M. S. Friedrich, J. K. Eckhardt, A. C. Wagner, N. Bohn, J. R. Binder, L. Chen, M. T. Elm, J. Janek, P. J. Klar, *ACS Energy Lett.* **2019**, *4*, 2117.
- [26] W. Jiang, C. Yin, Y. Xia, B. Qiu, H. Guo, H. Cui, F. Hu, Z. Liu, *ACS Appl. Mater. Interfaces* **2019**, *11*, 14023.
- [27] T. E. Ashton, P. J. Baker, C. Sotelo-Vazquez, C. J. M. Footer, K. M. Kojima, T. Matsukawa, T. Kamiyama, J. A. Darr, *J. Mater. Chem. A* **2021**, *9*, 10477.
- [28] R. Amin, Y.-M. Chiang, *J. Electrochem. Soc.* **2016**, *163*, A1512.
- [29] J. J. Kuo, S. D. Kang, W. C. Chueh, *Adv. Energy Mater.* **2022**, *12*, 2201114.
- [30] M.-J. Lee, E. Lho, P. Bai, S. Chae, J. Li, J. Cho, *Nano Lett.* **2017**, *17*, 3744.
- [31] N. Phattharasupakun, J. Wutthiprom, S. Duangdangchote, S. Sarawutanukul, C. Tomon, F. Duriyasart, S. Tubtimkuna, C. Aphirakaramwong, M. Sawangphruk, *Energy Storage Mater.* **2021**, *36*, 485.
- [32] Z. Du, D. L. Wood, C. Daniel, S. Kalnaus, J. Li, *J. Appl. Electrochem.* **2017**, *47*, 405.
- [33] Y. Kuang, C. Chen, D. Kirsch, L. Hu, *Adv. Energy Mater.* **2019**, *9*, 1901457.
- [34] M. Xu, B. Reichman, X. Wang, *Energy* **2019**, *186*, 115864.
- [35] [dataset], J. Naumann, N. Bohn, O. Birkholz, M. Neumann, M. Müller, J. R. Binder, M. Kamlah, **2023**, HierElecMorph; Zenodo, DOI 10.5281/zenodo.8337274.

Manuscript received: June 23, 2023

Revised manuscript received: September 15, 2023

Accepted manuscript online: September 18, 2023

Version of record online: ■ ■ ■ ■



**Hierarchically structured battery electrodes** offer short diffusion paths in the active material. We elucidate the impact of electrode morphology on the rate capability and discuss the

interplay between morphology and material properties. A careful design of the electrode is necessary to fully exploit the advantages of the hierarchical structure.

*J. Naumann\*, N. Bohn, Dr. O. Birkholz, Dr. M. Neumann, Dr. M. Müller, Dr. J. R. Binder, Prof. Dr. M. Kamlah\**

1 – 14

**Morphology-Dependent Influences on the Performance of Battery Cells with a Hierarchically Structured Positive Electrode**

